Quantitative analyses of high electroluminescence efficiency of thermally activated delayed fluorescence emitters based on acridine–triazine hybrids

Wei-Kai Lee
Yu-Hsin Huang
Kuan-Chung Pan
Ting-An Lin
Tanmay Chatterjee
Ken-Tsung Wong
Chung-Chih Wu

SPIE.

Quantitative analyses of high electroluminescence efficiency of thermally activated delayed fluorescence emitters based on acridine–triazine hybrids

Wei-Kai Lee,[a] Yu-Hsin Huang,[a] Kuan-Chung Pan,[a] Ting-An Lin,[a] Tanmay Chatterjee,[b] Ken-Tsung Wong,[b] and Chung-Chih Wu[a,c,d,]*

[a]National Taiwan University, Graduate Institute of Electronics Engineering, Taipei, Taiwan
[b]National Taiwan University, Institute of Atomic and Molecular Science Academia Sinica, Department of Chemistry, Taipei, Taiwan
[c]National Taiwan University, Department of Electrical Engineering, Taipei, Taiwan
[d]National Taiwan University, Graduate Institute of Photonics and Optoelectronics, Taipei, Taiwan

Abstract. Quantitative optical analyses were conducted on the mechanisms of impressively high electroluminescence (EL) efficiency (external quantum efficiency of up to 37%) achieved in previously reported blue organic light-emitting devices (OLEDs) using thermally activated delayed fluorescence emitters based on acridine–triazine hybrids. In addition to high photoluminescence quantum yields and preferentially horizontal emitting dipoles, optical simulation shows that the use of both low-index hole-transport layers (HTLs) and electron-transport layers (ETLs) also substantially contribute to enhanced optical outcoupling efficiencies and EL efficiencies of these devices. Further analyses on optical mode distributions and partitions in devices reveal significantly different optical outcoupling enhancement mechanisms for adopting low-index HTLs (i.e., reduced overall waveguided modes and enhanced microcavity effect) or adopting low-index ETLs (i.e., reduced surface plasmon and transverse magnetic waveguided modes), and their effects are combined to give even larger enhancement when reducing refractive indexes of both. Results of this work clearly indicate that optical properties of carrier-transport layers, in addition to their electrical properties, are critical factors and should also be carefully considered for future development of high-efficiency OLEDs. © *The Authors. Published by SPIE under a Creative Commons Attribution 3.0 Unported License. Distribution or reproduction of this work in whole or in part requires full attribution of the original publication, including its DOI.* [DOI: 10.1117/1.JPE.8.032105]

Keywords: organic light-emitting diodes; thermally activated delayed fluorescence; light extraction.

Paper 17121SS received Nov. 14, 2017; accepted for publication Feb. 5, 2018; published online Feb. 28, 2018.

1 Introduction

Advances of organic light-emitting diodes (OLEDs) and their display and lighting applications continuously impose requirements on high-efficiency materials and devices.[1–8] Since the pioneering introduction of thermally activated delayed fluorescence (TADF) emitters in OLEDs by Uoyama et al.,[2] TADF materials have attracted intensive research in the past few years. This is mainly due to the capability of TADF materials in harvesting triplet excitons by the thermally activated upconversion and in giving possible 100% internal quantum efficiency in electroluminescence (EL), through purely organic molecular frameworks and without the need to incorporate transition metals like in phosphorescent emitters.[1–8] In TADF molecules, through reducing the spatial overlap between the highest occupied molecular orbital and the lowest unoccupied molecular orbital, the energy gap (ΔE_{ST}) between the lowest excited singlet

(S_1) and triplet (T_1) states can be effectively reduced to facilitate efficient upconversion of T_1 excitons to S_1.[2,5–8] On the other hand, the optical outcoupling is also a critical issue for enhancing the overall external quantum efficiency (EQE) of OLEDs for practical use.[9,10] In addition to many other optical approaches and structures,[11–15] reports in recent years have revealed the importance of the emitting dipole orientations of OLED emitters relative to the device plane.[4,15–18] Horizontal emitting dipoles generate emission patterns (angular distributions of radiation) more suitable for direct outcoupling of internal light to the air, while radiation of vertical emitting dipoles couples strongly to waveguide (WG) modes and hugely to surface plasma (SP) modes for its transverse magnetic (TM) field-only nature. Since WG and SP modes are generally trapped and lost inside the OLED devices, preferentially horizontal dipole emitters having larger ratios of horizontal emitting dipoles that generally benefit higher-efficiency OLEDs (even without adopting any extra optical outcoupling techniques) have been intensively studied in recent years.

In our recent works,[19,20] we reported a series of efficient donor–acceptor (D-A) TADF emitters: SpiroAC-TRZ, DPAC-TRZ, DMAC-TRZ (Fig. 1) based on hybrids of the 2,4,6-triphenyl-1,3,5-triazine (TRZ) acceptor unit and the dimethyl, diphenyl, spirobiphenyl acridine donor units (DMAC, DPAC, SpiroAC). Some selected photophysical and EL properties of these TADF emitters doped in a bipolar and wide-triplet-energy host mCPCN [9-(3-(9H-carbazol-9-yl)phenyl)-9H-carbazole-3-carbonitrile] (12 wt.% doping concentration) are listed in Table 1. These acridine–triazine hyrbids are blue–green to sky blue emitters, all showing relatively small ΔE_{ST} of 62 to 133 meV, distinct TADF characteristics with delayed fluorescence lifetimes of 1.9 to 2.9 μs, high photoluminescence quantum yields (PLQYs) of 82% to 100%, preferentially horizontal emitting dipoles (with horizontal dipole ratios of 72% to 83%). Most importantly, these TADF emitters can be used to fabricate high-efficiency TADF OLEDs with high EQEs of 26% to 37%. Among these acridine–triazine hybrids, the sky–blue SpiroAC-TRZ gives particularly highest PLQY of ~100%, highest horizontal dipole ratio of 83%, and highest device EQE of ~37%. Although SpiroAC-TRZ possesses nearly ideal PLQY of ~100% and relatively high horizontal emitting dipole ratio of 83%, its very high device EQE of up to ~37% was still rather surprising. Although the horizontal emitting dipole ratio of 83% is high but not yet extremely high, the calculated optical outcoupling efficiency of up to ~38.3% in a
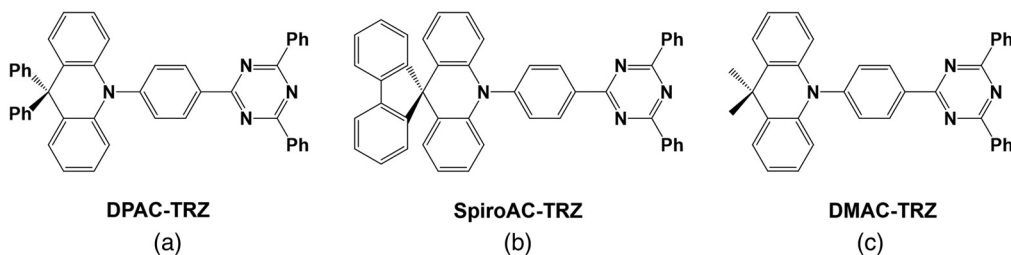

Fig. 1 Molecular structures for (a) DPAC-TRZ, (b) SpiroAC-TRZ, and (c) DMAC-TRZ.

Table 1 Selected photophysical and EL properties for acidine–triazine hybrid-based TADF emitters.

	$\Phi_{PL}{}^a$ (%)	$\theta_{//}{}^b$ (%)	$\phi_{out}{}^c$ (%)	$EQE_{max}{}^d$ (%)
DPAC-TRZ	82	78	35.7	25.8
SpiroAC-TRZ	100	83	38.3	36.7
DMAC-TRZ	90	72	33.1	26.5

aPhotoluminescence quantum yield.
bHorizontal emitting dipole ratio.
cCalculated optical outcoupling efficiency.
dMaximal EQE of the OLED device.

conventional planar OLED structure was also quite surprising.[20] Thus, detailed mechanisms of the very high optical outcoupling efficiencies and EL EQEs in our devices are certainly of interest. Here, we adopt the dipole-based electromagnetic model to quantitatively analyze and discuss the optical outcoupling efficiencies and EQEs in these TADF OLEDs.

2 Simulation Method

The simulation tool used for optical simulation of layer structures is developed by ourselves and is based on the equivalence between molecular emission through electronic dipole transitions and radiation from a classical electrical dipole antenna.[9,10,20] With the Fourier transformation of a dipole field into the k domain and the transfer matrix method to determine the properties of propagation, electromagnetic fields generated by a radiation dipole embedded in a layered structure are calculated, from which the distribution of the power density (dissipated to different modes) in each plane parallel to the device can be derived. The far-field intensity into substrate and into air is calculated by far-field approximation. Overall emission characteristics of an OLED are calculated by assuming that the emitting layer (EML) contains an ensemble of mutually incoherent dipole radiators with distributions in orientations, locations, and frequencies. The outcoupling efficiencies of internally generated radiation into air were calculated by locating emitting dipoles in the EML and by considering the orientational distribution ($\theta_{//}$) and the full spectral distribution of radiating dipoles. When calculating the pure optical outcoupling efficiency, the emitters are assumed to have 100% emission quantum efficiency.

3 Quantitative Analyses of High Electroluminescence Efficiencies

Efficient OLEDs based on these acridine–triazine hybrids adopted the general device structure of: glass substrate/indium tin oxide (ITO) (70 nm/MoO$_3$ (1 nm)/di-[4-(N, N-ditolyl-amino)-phenyl]-cyclohexane (TAPC) (y nm)/mCP (10 nm)/mCPCN doped with TADF dopants (12 wt.%, 20 nm)/3TPYMB (x nm)/LiF (0.5 nm)/Al (150 nm).[20] ITO and Al were anode and cathode, repsectiely. TAPC and N, N-dicarbazolyl-3,5-benzene (mCP) were hole-transport layers (HTL). The bipolar mCPCN host and TADF dopants constituted the EML. Tris-[3-(3-pyridyl)mesityl]borane (3TPYMB) was the ETL. MoO$_3$ and LiF were employed as hole and electron-injection layers (HIL, EIL). In calculating optical outcoupling efficiencies and overall emission characteristics, optical properties of various layers need to be input. In addition to the high PLQYs and preferentially horizontal emitting dipoles, we also noticed that the TAPC HTL and the 3TPYMB ETL have relatively low refractive indices (n), compared to many other HTL and ETL materials commonly used in OLEDs. Figure 2(a) shows the refractive index of TAPC, in comparison with those of several common HTL materials like NPB and TCTA, while Fig. 2(b) shows the refractive index of 3TPYMB, in comparison with those of several common ETL materials. It is seen that around the wavelengths of interest here (sky-blue to blue-green), various HTL and ETL materials could exhibit widely varied refractive indices, ranging from ~1.67 to ~1.93. Importantly, perhaps TAPC has the lowest n (~1.69) among various HTL materials and 3TPYMB has the lowest n (~1.67) among various ETL materials known in the literature. Lower refractive indices of active organic layers in OLEDs are in
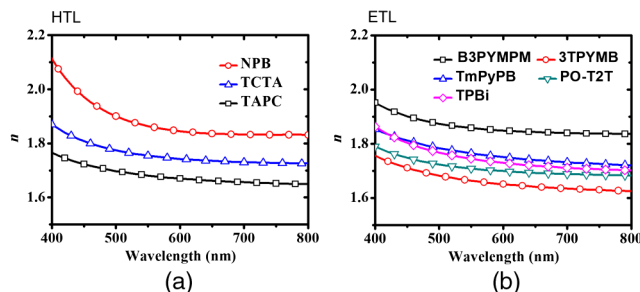

Fig. 2 Refractive indices of (a) various HTL materials and (b) various ETL materials.

general beneficial to OLED efficiencies, since the high refractive indices of OLED active layers are one of the major factors limiting optical outcoupling efficiencies. Several groups have shown that adoption of lower-refractive-index HIL, HTL, or ETL can enhance the light extraction efficiency of OLEDs.[21–26]

To investigate the influences of HTL refractive index (n_{HTL}) and ETL refractive index (n_{ETL}), we calculate the optical coupling/outcoupling efficiencies into air (ϕ_{air}) and into the substrate (ϕ_{sub}) for OLEDs adopting the DMAC-TRZ/DPAC-TRZ/SpiroAC-TRZ doped mCPCN EML and HTL/ETL of varied refractive indices, using the general device structure of: glass/ITO (70 nm)/HTL (x nm, n_{HTL})/EML (mCPCN:12 wt.% TADF emitter, 20 nm)/ETL (y nm, n_{ETL})/LiF/Al. The EML is assumed to have horizontal emitting dipole ratio $\theta_{//}$ and intrinsic emission spectrum of DMAC-TRZ (72%)/DPAC-TRZ (78%)/SpiroAC-TRZ (83%). Figures 3(a)–3(c) show calculated optimized ϕ_{air} for DMAC-TRZ/DPAC-TRZ/SpiroAC-TRZ devices as a function of n_{HTL} and n_{ETL}, while Figs. 3(d)–3(f) show calculated optimized ϕ_{sub} for DMAC-TRZ/DPAC-TRZ/SpiroAC-TRZ devices as a function of n_{HTL} and n_{ETL}. These optimized efficiencies are extracted from the first maximum value in varying x and y (HTL/ETL thicknesses) under certain n_{HTL} and n_{ETL}. Both ϕ_{air} and ϕ_{sub} monotonically increase as n_{HTL} and n_{ETL} decrease and as the horizontal emitting dipole ratio $\theta_{//}$ increases. It is seen that as both n_{HTL} and n_{ETL} decrease by 0.1, ϕ_{air} can increase by 4% to 6%. If both n_{ETL} and n_{HTL} can be lowered to 1.3, (ϕ_{air}, ϕ_{sub}) can reach ($\sim$62%, $\sim$90%) for SpiroAC-TRZ device (with higher $\theta_{//} = 83\%$ in EML) and ($\sim$58%, $\sim$88%) for DMAC-TRZ device (with lower $\theta_{//} = 72.\%$ in EML). In the actual devices using TAPC HTL ($n_{HTL} \sim 1.69$) and 3TPYMB ETL ($n_{ETL} \sim 1.67$), calculated (ϕ_{air}, ϕ_{sub}) for DMAC-TRZ/DPAC-TRZ/SpiroAC-TRZ devices are ($\sim$33%, $\sim$63%), ($\sim$35% to 36%, $\sim$69%), and ($\sim$38%, $\sim$70%), respectively. These results well support the very high EQE of $\sim$37% achieved for the planar SpiroAC-TRZ device and high EQE of $\sim$63% achieved when attached with extraction lens to the substrate.[20]

To further investigate the mechanism of high optical outcoupling efficiency, the power densities (or the mode distribution) as a function of k_t/k_o for the SpiroAC-TRZ based device (at the PL peak wavelength) under different n_{HTL}/n_{ETL} conditions are simulated and are shown in Fig. 4, where k_t is the transverse component of the wavenumber (i.e., along the device plane) and k_o is the wavenumber in vacuum. Figure 4(a) shows the calculated power densities for fixed $n_{HTL} = 1.8$ and varied n_{ETL} from 2.0 to 1.3, in which various modes such as the
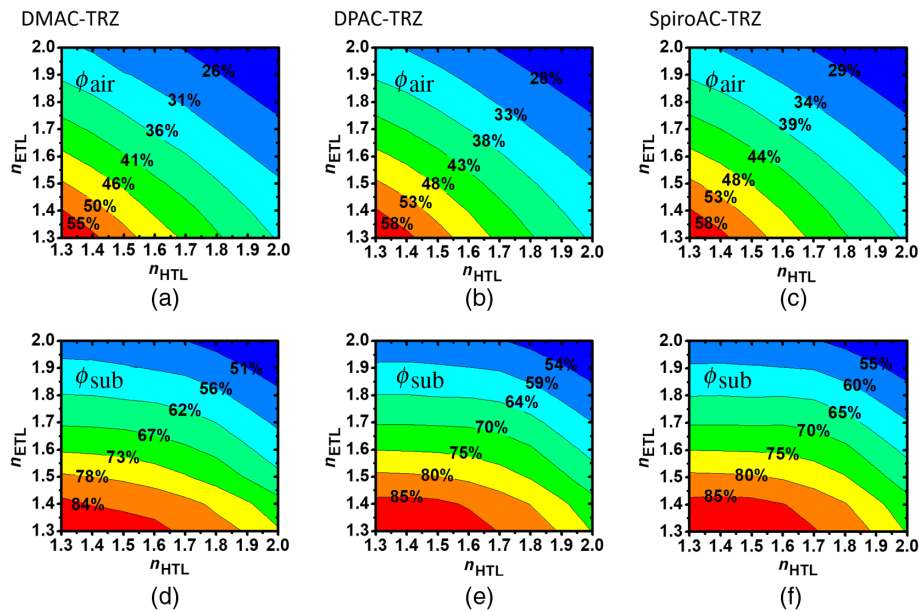

Fig. 3 Calculated coupling efficiency into air ϕ_{air} for (a) DMAC-TRZ, (b) DPAC-TRZ, and (c) SpiroAC-TRZ, and calculated coupling efficiency into substrate ϕ_{sub} for (d) DMAC-TRZ, (e) DPAC-TRZ, and (f) SpiroAC-TRZ.

$n_{HTL} = 1.8$ $\qquad\qquad$ $n_{ETL} = 1.8$ $\qquad\qquad$ $n_{HTL} = n_{ETL} = n_{org}$
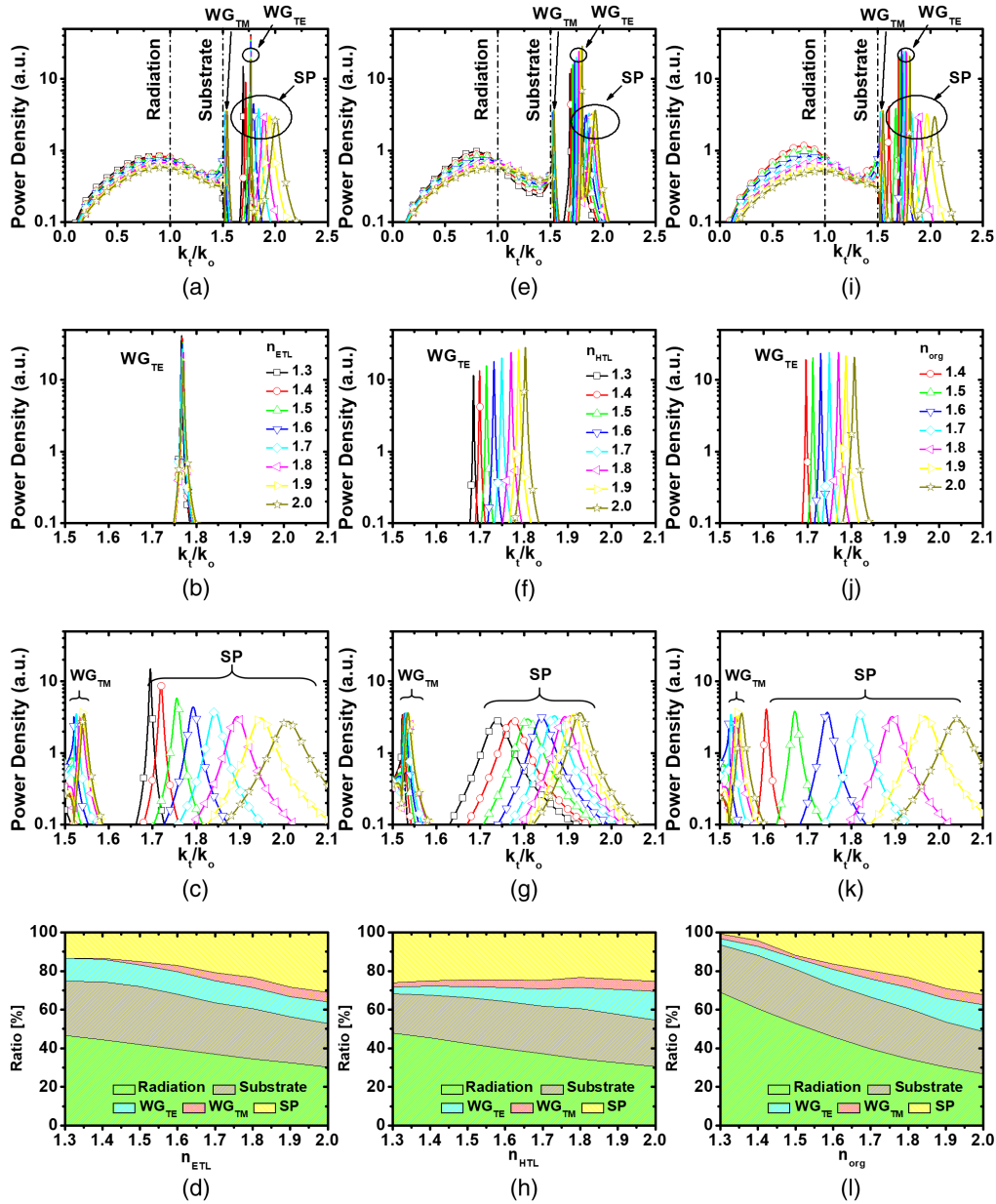

Fig. 4 (a)–(d) Calculated mode distributions and fraction ratios for the devices with varied n_{ETL} and fixed $n_{HTL} = 1.8$: (a) overall mode distributions, (b) the TE component in the range of $k_t/k_o = 1.5$ ~2.1, (c) the TM component in the range of $k_t/k_o = 1.5$ ~2.1, and (d) fraction ratios of various modes. (e)–(h) Calculated mode distributions and fraction ratios for the devices with varied n_{HTL} and fixed $n_{ETL} = 1.8$: (e) overall mode distributions, (f) the TE component in the range of $k_t/k_o = 1.5$ ~2.1, (g) the TM component in the range of $k_t/k_o = 1.5$ ~2.1, and (h) fraction ratios of various modes. (i)–(l) Calculated mode distributions and fraction ratios for the devices with varied $n_{org} = n_{HTL} = n_{ETL}$: (i) overall mode distributions, (j) the TE component in the range of $k_t/k_o = 1.5$ ~2.1, (k) the TM component in the range of $k_t/k_o = 1.5$ ~2.1, and (l) fraction ratios of various modes (each distribution is normalized by area).

radiation modes, substrate modes, TM waveguided modes (WG$_{TM}$), transverse electric (TE) waveguided modes (WG$_{TE}$), and surface plasmon modes (SP, which is of TM nature) can be seen and assigned. As n_{ETL} decreases from 2.0 to 1.3, the SP peak shifts substantially from $k_t/k_o = 2.01$ to 1.7. Since such a shift would lead to overlap of SP modes with WG$_{TE}$ modes (roughly fixed around $k_t/k_o \sim 1.77$) in some cases, TE and TM components of the

power densities for the selected range of $k_t/k_o = 1.5$ to 2.1 for various n_{ETL}, are depicted separately in Figs. 4(b) and 4(c), respectively, so that WG_{TE} and SP parts (and also WG_{TM}) can be more clearly distinguished. As seen in Fig. 4(c), in addition to the peak shift, the SP band also narrows significantly (thus integrated areas decrease) when lowering n_{ETL}, which is beneficial for reducing the SP loss and for enhancing the optical outcoupling efficiency. The WG_{TM} band (around $k_t/k_o = 1.5$ to 1.6) also shows a similar shift toward smaller k_t/k_o and narrowing (although less significantly). By contrast, the WG_{TE} band position and width [Fig. 4(b)] are more or less fixed around $k_t/k_o = 1.77$. The fraction ratios of various modes are shown in Fig. 4(d). While ratios of both SP and WG_{TM} modes decrease with lower n_{ETL}, the ratio of WG_{TE} modes roughly remains constant. Thus, both increased radiation mode ratios (i.e., enhanced optical outcoupling) and substrate mode ratios with lower n_{ETL} observed in Figs. 4(a) and 4(d) can mainly be attributed to reduction of SP and WG_{TM} modes.

Figures 5(a) and 5(b) show the distributions of field intensities (electric field E for the WG_{TE} mode and magnetic field H for WG_{TM} and SP modes) for the modes corresponding to WG_{TE}, WG_{TM}, and SP peaks for the OLED having typical high n_{HTL}/high $n_{ETL} = 1.8/1.8$ and for the OLED having high n_{HTL}/low $n_{ETL} = 1.8/1.5$. For typical OLEDs having high n_{HTL}/high n_{ETL}, the WG_{TE} mode mainly distributes in ITO and HTL; the WG_{TM} mode distributes around both the metal/ETL interface and the ITO/substrate interface; the SP mode peaks at the metal/ETL interface and decays toward the substrate. With reduced n_{ETL}, the field distribution of the SP mode shifts more toward the ITO from the metal interface because the relatively high n of HTL and ITO tends to attract the field/photon energy, forming a more WG-like SP mode (or WG-SP hybrid mode). Comparison of Figs. 5(a) and 5(b) also reveals more similar field distributions for WG_{TE} modes at $k_t/k_o = 1.77$, which is understandable since WG_{TE} modes are roughly confined in ITO and high-n HTL and the variation of n_{ETL} would less influence their field distributions and k_t/k_o peak positions. On another note, for the case of low n_{ETL} and high n_{HTL}, the electromagnetic fields in the device are more confined in ITO and HTL, which might be useful for obtaining effective light extraction by some internal light extraction structures near/within ITO.

Similarly, Figs. 4(e)–4(h) show the overall power densities, TM and TE components of the power densities for the selected range of $k_t/k_o = 1.5$ to 2.0, and the fraction ratios of various modes, respectively, for fixed $n_{ETL} = 1.8$ and varied n_{HTL} from 2.0 to 1.3. The SP peaks also shift toward smaller k_t/k_o as n_{HTL} decreases [Fig. 4(g)], but the shift is smaller compared to those in Fig. 4(c). The shift of SP peaks toward smaller k_t/k_o upon reducing n_{HTL} and n_{ETL} in general is due to lower effective refractive indices of the dielectric layers in front of the metal surface. The larger shift with reduced n_{ETL} than with reduced n_{HTL} is because the ETL is more adjacent to the metal layer. Also, the integrated areas of SP modes [also the fraction ratio of SP modes in Fig. 4(h)] do not change evidently when n_{HTL} varies, thus not contributing to enhancement of optical outcoupling efficiency. Meanwhile, both WG_{TE} and WG_{TM} modes shift toward smaller k_t/k_o as n_{HTL} decreases. In addition to the peak shift, their bandwidths and intensities also drop
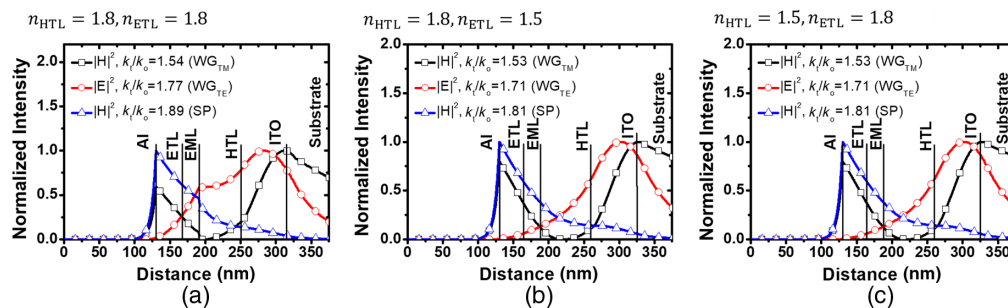

Fig. 5 The spatial distributions (along the device vertical direction) of the field intensities (TE field E_y or TM field H_y) in the device for the WG_{TE} mode, the WG_{TM} mode, and the SP mode for devices having (a) $n_{HTL} = 1.8$ and $n_{ETL} = 1.8$, (b) $n_{HTL} = 1.8$ and $n_{ETL} = 1.5$, and (c) $n_{HTL} = 1.5$ and $n_{ETL} = 1.8$.

(thus reduced integrated areas) when n_{HTL} lowers, resulting in reduction of both trapped WG modes, as clearly indicated in Fig. 4(h). This reduction of trapped WG modes is the main contributor to the enhancement of ϕ_{sub} by ~8% [Fig. 3(f)] as n_{HTL} decreases from 2.0 to 1.3 (while n_{ETL} fixed at 1.8). However, it cannot fully account for the significantly larger increase of ϕ_{air} by ~14% to 16% [Fig. 3(c)] as n_{HTL} decreases from 2.0 to 1.3 (while n_{ETL} fixed at 1.8). In Fig. 4(e), one notices that, as n_{HTL} decreases, not only the overall radiation coupling into the substrate (i.e., radiation + substrate modes) increases but also its distribution shifts toward to smaller k_t/k_o (i.e., larger ratio of radiation is relocated into smaller angles for direct outcoupling), resulting in larger ϕ_{air} enhancement over the overall ϕ_{sub} enhancement [as also clearly seen in Fig. 4(h)]. This more concentrated angular distribution (in the substrate) is associated with the enhanced microcavity effect resulting from the increased index difference and optical reflection between the high-n ITO and the low-n HTL (thus like a pair of dielectric mirror). Indeed, the calculated reflectance spectra for the complete OLED with different n_{HTL} (n_{ETL} fixed at 1.8), as shown in Fig. 6, clearly exhibit stronger resonance for lower n_{HTL}. Figure 5(c) shows the distributions of field intensities for the modes corresponding to WG_{TE}, WG_{TM}, and SP peaks for the OLED having low n_{HTL}/high $n_{ETL} = 1.5/1.8$. Comparison of Figs. 5(a) and 5(c) reveals that the field distributions of WG_{TM} and SP modes remain similar but WG_{TE} becomes more concentrated in ITO when n_{HTL} decreases.

Since in the high-efficiency SpiroAC-TRZ devices, both the HTL (TAPC) and ETL (3TPYMB) have similarly low refractive indexes ($n < 1.7$), we have also analyzed mode properties for the case of $n_{ETL} = n_{HTL} = n_{org}$. Figures 4(i)–4(l) show the overall power densities, TM and TE components of the power densities for the selected range of $k_t/k_o = 1.5$ to 2.0, and the fraction ratios of various modes, respectively, for varied $n_{ETL} = n_{HTL} = n_{org}$ from 2.0 to 1.4. In reducing $n_{ETL} = n_{HTL} = n_{org}$, mode properties shown in Figs. 4(j)–4(k) appear to combine features seen for cases of low-n HTL and low-n ETL. All the SP, WG_{TE}, and WG_{TM} bands shift toward smaller k_t/k_o and narrow significantly. As a result, fraction ratios of SP, WG_{TE}, and WG_{TM} modes all drop with $n_{org} = n_{ETL} = n_{HTL}$, together contributing to even more significant enhancement of substrate + radiation modes [see Figs. 3(f), 4(i), and 4(l)]. Interestingly, the fraction ratio of substrate modes remains more or less constant in reducing n_{org} [Figs. 4(i) and 4(l)], and reduction of SP, WG_{TE}, and WG_{TM} modes indeed mainly leads to enhancement of the radiation modes that can be directly outcoupled (i.e., enhancement of ϕ_{out}). As $n_{org} = n_{ETL} = n_{HTL}$ decreases, in Fig. 4(i), one again observes more concentrated angular distribution of radiation coupled into the substrate (within smaller angles, i.e., at $k_t/k_o \leq 1$), more readily for direct outcoupling. This more concentrated angular distribution (in the substrate) is again associated with the enhanced microcavity effect resulting from the increased index difference and optical reflection between the high-n ITO and the low-n HTL. Thus, intriguingly, upon reducing both n_{ETL} and n_{HTL}, the enhancement of optical outcoupling is not only from reduced SP/WG_{TE}/WG_{TM} modes (due to low-n HTL/ETL) but also from enhanced microcavity effect and more angularly concentrated distribution in the substrate. These together give even more significant enhancement of optical outcoupling compared to the simply low-n ETL or low-n HTL case.
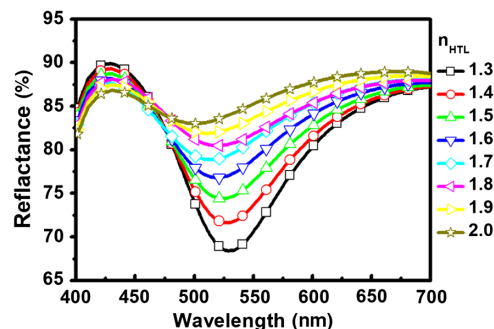

Fig. 6 The reflectance spectra of devices with $n_{ETL} = 1.8$ and varied n_{HTL}.

4 Conclusion

In summary, we had used the dipole-based electromagnetic model to quantitatively analyze why the surprisingly high EQE of ~37% can be achieved in previously reported OLEDs using TADF emitters based on the acridine–triazine hybrids. It is found that in addition to the high PLQYs and preferentially horizontal emitting dipoles, the use of low-index HTLs and ETLs also substantially help enhance the optical outcoupling efficiencies and EQEs of the devices. Although lowering refractive indices of either HTLs or lowering those of ETLs are both similarly effective to enhance OLED optical outcoupling efficiency, detailed enhancement mechanisms are different. The enhancement of optical outcoupling with low-index ETLs is mainly due to reduced SP modes and TM waveguided modes that are more affected by the refractive index of ETLs. On the other hand, the enhancement with low-index HTLs is due to reduced WG modes (both TE and TM modes that are affected by the refractive index of HTLs) and also enhanced microcavity effect that causes more angularly concentrated radiation more readily for direct outcoupling. Most importantly, when reducing refractive indexes of both HTLs and ETLs, all these mechanisms (reduced SP/TE/TM modes, microcavity effect) combine together to give even more significant enhancement in optical outcoupling. In general, upon reducing refractive indexes of both by 0.1, optical outcoupling efficiencies can increase by 4% to 6%. Results of this work should be useful for better understanding the material design and device architecture for highly efficient OLEDs and also clearly indicate that both electrical and optical properties of carrier-transport layers should be carefully considered for future development of high-efficiency OLEDs.

Acknowledgments

References

1. M. A. Baldo et al., "Highly efficient phosphorescent emission from organic electroluminescent devices," *Nature* **395**, 151–154 (1998).
2. H. Uoyama et al., "Highly efficient organic light-emitting diodes from delayed fluorescence," *Nature* **492**, 234–238 (2012).
3. H. Sasabe et al., "Recent progress in phosphorescent organic light-emitting devices," *Eur. J. Org. Chem.* **2013**, 7653–7663 (2013).
4. C.-Y. Kuei et al., "Bis-tridentate Ir(III) complexes with nearly unitary RGB phosphorescence and organic light-emitting diodes with external quantum efficiency exceeding 31%," *Adv. Mater.* **28**, 2795–2800 (2016).
5. Y. J. Cho et al., "20% external quantum efficiency in solution-processed blue thermally activated delayed fluorescent devices," *Adv. Funct. Mater.* **25**(43), 6786–6792 (2015).
6. W.-C. Chen et al., "Blue-emitting organic electrofluorescence materials: progress and prospective," *J. Mater. Chem. C* **3**, 10957–10963 (2015).
7. K. Shizu et al., "Highly efficient electroluminescence from purely organic donor-acceptor systems," *Pure Appl. Chem.* **87**, 627–638 (2015).
8. Y. Tao et al., "Thermally activated delayed fluorescence materials towards the breakthrough of organoelectronics," *Adv. Mater.* **26**, 7931–7958 (2014).
9. C.-L. Lin et al., "Enhancing light outcoupling of organic light-emitting devices by locating emitters around the second antinode of the reflective metal electrode," *Appl. Phys. Lett.* **88**, 081114 (2006).
10. K. Neyts, "Microcavity effects and the outcoupling of light in displays and lighting applications based on thin emitting films," *Appl. Surf. Sci.* **244**, 517–523 (2005).
11. Y. Sun et al., "Organic light emitting devices with enhanced outcoupling via microlenses fabricated by imprint lithography," *J. Appl. Phys.* **100**, 073106 (2006).
12. H.-W. Chang et al. "Nano-particle based scattering layers for optical efficiency enhancement of organic light-emitting diodes and organic solar cells," *J. Appl. Phys.* **113**, 204502 (2003).

13. Y. R. Do et al. "Enhanced light extraction from organic light-emitting diodes with 2D SiO_2/SiN_x photonic crystals," *Adv. Mater.* **15**, 1214–1218 (2003).
14. J. Feng, T. Okamoto, and S. Kawata, "Highly directional emission via coupled surface-plasmon tunneling from electroluminescence in organic light-emitting devices," *Appl. Phys. Lett.* **87**, 241109 (2005).
15. C.-Y. Chen et al. "Enhancing optical out-coupling of organic light-emitting devices with nanostructured composite electrodes consisting of indium tin oxide nanomesh and conducting polymer," *Adv. Mater.* **27**, 4883–4888 (2015).
16. J. W. Sun et al., "A fluorescent organic light-emitting diode with 30% external quantum efficiency," *Adv. Mater.* **26**, 5684–5688 (2014).
17. H. Kaji et al., "Purely organic electroluminescent material realizing 100% conversion from electricity to light," *Nat. Commun.* **6**, 8476 (2015).
18. C. Mayr et al., "Efficiency enhancement of organic light-emitting diodes incorporating a highly oriented thermally activated delayed fluorescence emitter," *Adv. Funct. Mater.* **24**, 5232–5239 (2014).
19. W.-L. Tsai et al., "A versatile thermally activated delayed fluorescence emitter for both highly efficient doped and non-doped organic light emitting devices," *Chem. Commun.* **51**, 13662–13665 (2015).
20. T.-A. Lin et al., "Sky-blue organic light emitting diode with 37% external quantum efficiency using thermally activated delayed fluorescence from spiroacridine-triazine hybrid," *Adv. Mater.* **28**, 6976–6983 (2016).
21. Y.-H. Huang et al., "Unlocking the full potential of conducting polymers for high-efficiency organic light-emitting devices," *Adv. Mater.* **27**, 929–934 (2015).
22. M. Jiao et al., "Simple planar indium-tin-oxide-free organic light-emitting devices with nearly 39% external quantum efficiency," *Adv. Opt. Mater.* **4**, 365–370 (2016).
23. C.-Y. Lu et al., "Achieving above 60% external quantum efficiency in organic light-emitting devices using ITO-free low-index transparent electrode and emitters with preferential horizontal emitting dipoles," *Adv. Funct. Mater.* **26**, 3250–3258 (2016).
24. H. Shin et al., "Blue phosphorescent organic light-emitting diodes using an exciplex forming co-host with the external quantum efficiency of theoretical limit," *Adv. Mater.* **26**, 4730–4734 (2014).
25. H. Shin et al., "Sky-blue phosphorescent OLEDs with 34.1% external quantum efficiency using a low refractive index electron transporting layer," *Adv. Mater.* **28**, 4920–4925 (2016).
26. C. Fuchs et al., "Enhanced light emission from top-emitting organic light-emitting diodes by optimizing surface plasmon polariton losses," *Phys. Rev. B* **92**, 245306 (2015).

Wei-Kai Lee is currently a PhD student at Graduate Institute of Electronics Engineering, National Taiwan University (NTU), Taiwan. He received his MS degree in the Graduate Institute of Electronics Engineering, NTU, in 2015 and his BS degree in the Department of Electrical Engineering, NTU, in 2013. His research fields include OLED devices, OLED optics and modeling, optical, and photophysical properties of OLED materials, and related device/display technologies.

Biographies for the other authors are not available.